Research Article Vol. 6, No. 3 / March 2019 / Optica 354

Strong coupling of ionizing transitions

Erika Cortese,[1] Iacopo Carusotto,[2] Raffaele Colombelli,[3] and Simone De Liberato[1,*]

[1]School of Physics and Astronomy, University of Southampton, Southampton, SO17 1BJ, UK
[2]INO-CNR BEC Center and Dipartimento di Fisica, Universita di Trento, I-38123 Povo, Italy
[3]Centre de Nanosciences et de Nanotechnologies, CNRS UMR 9001, Université Paris-Sud, Université Paris-Saclay, C2N - Orsay, 91405 Orsay cedex, France
*Corresponding author: S.De-Liberato@soton.ac.uk

Received 29 November 2018; revised 23 January 2019; accepted 24 January 2019 (Doc. ID 353148); published 11 March 2019

In cavity quantum electrodynamics, strong light–matter coupling is normally observed between a photon mode and a discrete optically active transition. In the present work we demonstrate that strong coupling can also be achieved using ionizing, intrinsically continuum, transitions. This leads to the appearance of novel discrete polaritonic resonances, corresponding to dressed bound exciton states, kept together by the exchange of virtual cavity photons. We apply our theory to the case of intersubband transitions in doped quantum wells, where Coulomb-bound excitons are absent. In considering quantum wells with a single bound electronic subband, in which all transitions involve states in the continuum, we find that the novel bound excitons predicted by our theory are observable within present-day, realistic parameters. Our work shows how strong light–matter coupling can be used as a novel gauge to tune both optical and electronic properties of semiconductor heterostructures beyond those permitted by mere crystal properties.

https://doi.org/10.1364/OPTICA.6.000354

1. INTRODUCTION

When a single photon can be trapped in an optical resonator long enough to undergo multiple absorption and re-emission cycles, the coupled light–matter system is said to be in the strong coupling regime. Its physics cannot then be correctly described in terms of irreversible absorption and emission of photons; instead it becomes necessary to consider hybrid quasiparticles, half-light half-matter, named polaritons [1]. Many works have demonstrated how the hybridization with matter strongly alters not only the spectrum, but also the field profile [2–4], and the quantum [5–8] and nonlinear [9,10] properties of the photonic resonator. More recently, interest has also broadened toward investigating how strong coupling can be used to modify properties of the underlying matter degrees of freedom [11–19], including changes in electrical [20–23] and photochemical [24–26] properties.

Notwithstanding a large and rapidly growing interest in polaritonic physics, until now the only transitions exploited to achieve strong coupling were those between bound electronic states. Bound-to-continuum ionizing transitions would in fact seem to be, by their very nature, irreversible, as the ionized components get separated upon photon absorption, thus not allowing for a subsequent re-emission.

In this work we demonstrate that ionizing electronic transitions can be strongly coupled to a photonic resonator, leading to the appearance of discrete polaritonic resonances below the ionization threshold. The electronic part of such resonances corresponds to bound excitons not present in the uncoupled system, and are thus generated by the coupling with the cavity-photonic field. In particular, these bound states do not rely on the Coulomb attraction between electrons and holes underlying standard excitons. Apart from its importance from a fundamental perspective, this discovery opens the way to a number of practical applications, as those novel bound states can be pathways for chemical reactions, improve the efficiency of multi-photon transitions, or push the tunability of semiconductor devices beyond that allowed by mere electronic properties.

Most of the concepts introduced in this paper are general enough to be broadly applied to any cavity quantum electrodynamics platform, including atomic and molecular systems, for which quantum electrodynamics density-functional approaches are currently being developed [27,28]. Notwithstanding the above, henceforth we will consider the specific case of microcavity-embedded doped quantum wells, sketched in Fig. 1, which have an immediate technological relevance while also allowing for a simpler and more transparent theoretical treatment thanks to their effective one-dimensional nature. In those systems the confinement along the growth (z) axis splits the conduction band into multiple discrete bound or continuous unbound subbands. The parabolic quasi-parallel in-plane dispersion then allows for the excitation of resonant coherent electronic transitions with long dephasing times. When more than one bound subband is present, the resulting narrow optical transition has been successfully strongly coupled with mid-infrared and terahertz resonators [29–31]. The resulting quasiparticles, named intersubband polaritons, have been highlighted as a promising platform for long-wavelength optoelectronics [32–35], with the possibility

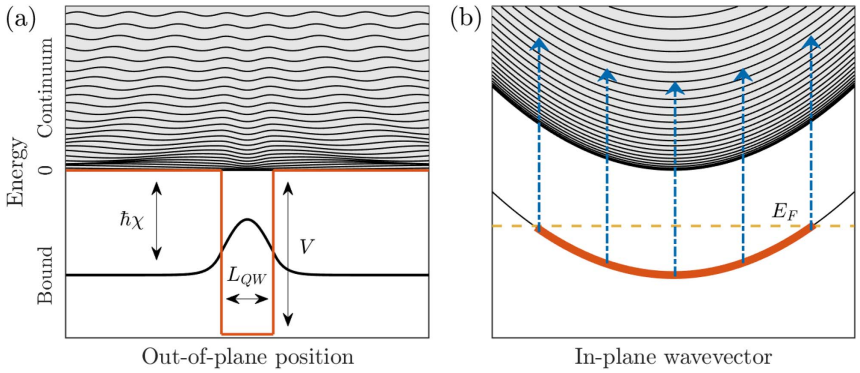

Fig. 1. Schematic representation of the electronic structure of a quantum well of width L_{QW}, with a single bound state below the continuum (shaded in gray). (a) Electronic density envelope functions of the different single-particle eigenmodes, shifted by their energy. The potential profile is plotted in red, with the first ionization energy $\hbar\chi$ and the conduction band discontinuity V explicitly marked. The figure has been obtained using the parameters of the structure described in Section 3.A. For sake of clarity, only one continuum mode in every 10 is shown, with its density multiplied by 10. (b) In-plane dispersion of the different subbands in momentum space. The single bound state is filled with electrons (in red), up to the Fermi energy E_F (dashed yellow line). The dashed–dotted blue arrows represent a collective bound-to-continuum transition.

of tuning the doping *in situ* by optical or electrical means [36,37]. The role of intersubband polariton formation on the electronic wavefunction has been investigated in the past [38], highlighting the possibility of dramatically increasing the emission efficiency by injecting electrons into superradiant bright states. Bound-to-continuum transitions in doped quantum wells have also been the object of theoretical [39] and experimental [40] investigations.

2. THEORY

In this section we will sketch the theory of the bound-to-continuum strong coupling and the calculation of the corresponding resonator-induced bound excitonic states. Detailed derivations can be found in Supplement 1.

A. Spectrum

The problem of the coupling between a discrete resonance (in our case the photonic mode) and a continuum (the bound-to-continuum electronic transitions) was initially treated by Fano in his landmark paper [41]. In such a work, the coupled eigenfrequencies are always assumed to fall into the uncoupled continuum, leading to the characteristic asymmetric broadened absorption lineshape. The limit of a very narrow continuum, describing an inhomogeneously broadened discrete resonance, has also been investigated [42,43]. Here we will instead consider the case of a semi-infinite ionization continuum of unbound states, in which one of the hybridized light–matter eigenmodes lies below its lowest edge. This can happen either because the uncoupled discrete resonance is not resonant with the continuum to start with, or because the coupling is large enough to *push* a coupled eigenmode out of the continuum.

In a planar semiconductor heterostructure, the electronic states can be indexed by the in-plane two-dimensional momentum vector $\mathbf{k}$ and by an index n, which runs over both bound and continuum states quantized along the growth, out-of-plane axis. The field operator for electrons of in-plane momentum $\mathbf{k}$ can thus be written as

$$\Psi_{\mathbf{k}}(z) = \sum_n \phi_n(z) c_{n\mathbf{k}}, \tag{1}$$

where $c_{n\mathbf{k}}$ is the fermionic annihilation operator of the nth electron level with in-plane wavevector $\mathbf{k}$, frequency $\omega^c_{n\mathbf{k}}$, and envelope wavefunction $\phi_n(z)$. The electronic single-particle spectrum will be characterized by one or more bound levels $\omega^c_{n\mathbf{k}} < 0$, and a series of unbound states delocalized across the bulk $\omega^c_{n\mathbf{k}} > 0$. Those states can either form a real continuum or arrange themselves in a set of broadened minibands, depending on the details of the potential felt by the electrons. We will in the following use the term *continuum* with the understanding that it can cover both situations.

Collective electronic transitions between single-particle states can be indexed by the in-plane wavevector $\mathbf{q}$ and the index $\alpha \equiv (nm)$, with m and n, respectively, the initial and final electronic levels. Narrowing down to the case of interest, we consider a system in which only bound-to-continuum transitions are optically active, by choosing the number of electrons N such that, as depicted in Fig. 1(b), the Fermi energy stands between the bottom of the last bound and first unbound subbands. A cavity photon with in-plane wavevector $\mathbf{q}$ thus couples to electronic transitions described by the dipole operators:

$$b^\dagger_{(nm)\mathbf{q}} = \frac{1}{\sqrt{N}} \sum_{\mathbf{k}} c^\dagger_{n\mathbf{k}+\mathbf{q}} c_{m\mathbf{k}}. \tag{2}$$

In the dilute excitation regime, in which the number of excitations in the system is much smaller than N, those operators satisfy bosonic commutation relations [32,44,45]:

$$[b_{\alpha\mathbf{q}}, b^\dagger_{\beta\mathbf{q}'}] = \delta_{\alpha\beta}\delta(\mathbf{q}-\mathbf{q}'). \tag{3}$$

Many-body plasmonic effects can become important at high doping densities. The Hamiltonian describing single particle transitions $b_{\alpha\mathbf{q}}$, and their mutual Coulombic interaction, can then be diagonalized through a Bogoliubov rotation, leading to a Hamiltonian of decoupled multisubband plasmon modes $p_{\alpha\mathbf{q}}$ [46–49]. The Bogoliubov rotation can then be inverted, writing the single particle transition operators as linear superpositions of the plasmonic ones:

$$(b^\dagger_{\alpha\mathbf{q}} + b_{\alpha-\mathbf{q}}) = \sum_\beta h_{\alpha\beta}(p^\dagger_{\beta\mathbf{q}} + p_{\beta-\mathbf{q}}). \tag{4}$$

By introducing $a^\dagger_{\mathbf{q}}$, the bosonic creation operator for a cavity photon of in-plane wavevector $\mathbf{q}$ and frequency $\omega^a_{\mathbf{q}}$, the light–matter Hamiltonian takes the form

$$H = \sum_{\mathbf{q}} \Bigg[\hbar\omega_q^a a_{\mathbf{q}}^\dagger a_{\mathbf{q}} + \sum_\alpha \hbar\omega_\alpha^p p_{\alpha\mathbf{q}}^\dagger p_{\alpha\mathbf{q}} + \sum_\alpha \frac{\hbar\Xi_{\alpha q}}{2} (a_{-\mathbf{q}}^\dagger + a_{\mathbf{q}})(p_{\alpha\mathbf{q}}^\dagger + p_{\alpha-\mathbf{q}}) \Bigg],$$

where ω_α^p are the frequencies of the electronic transitions dressed by local-field effects and $\Xi_{\alpha q}$ is the renormalized light–matter coupling. This Hamiltonian can be diagonalized in terms of bosonic hybrid light–matter polariton operators:

$$d_{s\mathbf{q}} = x_{sq} a_{\mathbf{q}} + z_{sq} a_{-\mathbf{q}}^\dagger + \sum_\alpha [y_{s\alpha q} p_{\alpha\mathbf{q}} + w_{s\alpha q} p_{\alpha-\mathbf{q}}^\dagger]. \quad (5)$$

When the index s runs over solutions that are in the continuum, the system is equivalent to that described by Fano, and we will not explicitly discuss its solution here. We consider instead solutions with frequency $\omega_{sq}^d < \chi$, where we define the frequency of first ionization χ as the lowest ω_α^p belonging to a continuum part of the spectrum [see Fig. 1(a)]. The discrete nature of those polaritonic modes implies their matter component is a bound excitonic state generated by the coupling with the photonic field. This novel mechanism of binding is to be contrasted to the usual Coulomb electron–hole interaction that binds standard excitons. The eigenvalue ω_{sq}^d is shown (in this case) to obey the eigenequation (see Supplement 1)

$$\frac{\omega_q^a}{\omega_q^{a2} - \omega_{sq}^{d2}} \sum_\alpha \frac{|\Xi_{\alpha q}|^2 \omega_\alpha^p}{\omega_\alpha^{p2} - \omega_{sq}^{d2}} = 1. \quad (6)$$

The existence of a solution satisfying Eq. (6) can be easily proved if the photonic mode lies below the frequency of first ionization ($\omega_q^a < \chi$). In the opposite case ($\omega_q^a > \chi$), however, one needs to solve the integral equation to verify whether the interaction is strong enough to *push* the hybrid light–matter mode out of the continuum.

B. Excitonic States

Assuming for the moment that Eq. (6) has at least a solution $\omega_{sq}^d < \chi$, we will now study its properties. The operator in Eq. (5) describes the normal mode of the system as a superposition of photonic and matter excitations but, notwithstanding the fact all electronic transitions are in the continuum, and thus all the available final states unbound, there is not enough energy to promote an electron to an unbound state. The particular linear superposition of bound-to-continuum transitions specified by the $y_{s\alpha q}$ and $w_{s\alpha q}$ coefficients in Eq. (5) thus has to describe a bound excitonic state not present in the uncoupled Hamiltonian. To visualize such a state we can define the electron density,

$$N(z) = \sum_{\mathbf{k}} \Psi_{\mathbf{k}}^\dagger(z) \Psi_{\mathbf{k}}(z), \quad (7)$$

and calculate its difference between the ground state $|G\rangle$ and the state with one excitation in an arbitrary $d_{s\mathbf{q}}$ polaritonic mode:

$$\begin{aligned} \Delta N_{s\mathbf{q}}(z) &= \langle G | d_{s\mathbf{q}} N(z) d_{s\mathbf{q}}^\dagger | G \rangle - \langle G | N(z) | G \rangle \\ &= P_{sq} [|\psi_{sq}^e(z)|^2 - |\psi_{sq}^g(z)|^2], \end{aligned} \quad (8)$$

where, P_{sq} is the weight of the matter component of the polaritonic mode, and $\psi_{sq}^g(z)$ and $\psi_{sq}^e(z)$, built respectively only by wavefunctions of initially full and empty electronic levels, can be interpreted as the wavefunctions of the initial (ground) and final (excited) states of the excitonic transition created by the operator $d_{s\mathbf{q}}^\dagger$.

3. RESULTS

We will now apply the previously developed theory to the case of n_{QW} identical doped GaAs/Al_xGa_{1-x}As quantum wells of width $L_{\mathrm{QW}} = 4$ nm. The Al fraction $x = 0.33$ then ensures that each quantum well will have a single electronic bound state. Intersubband polaritons have been demonstrated in those structures, with doping levels up to $N_{\mathrm{2DEG}} = 3 \times 10^{12}$ cm^{-2} [35]. Electronic bare wavefunctions are then calculated considering a single conduction band in the effective mass approximation and using Bastard boundary conditions for the envelope functions [50]. These eigenfunctions are used to calculate all the electronic parameters of Eq. (5). The resulting multi-mode Hopfield matrix is then numerically diagonalized, leading to the determination of the eigenfrequencies ω_{sq}^d and of the eigenvectors in Eq. (5). Those coefficients are then used in Eq. (8) to calculate the ground and excited electronic densities $|\psi_{sq}^g(z)|^2$ and $|\psi_{sq}^e(z)|^2$, and the matter weight P_{sq}.

A. $n_{\mathrm{QW}} = 1$

To build a good understanding of the implications of bound-to-continuum strong coupling, we start by considering a single quantum well in a wide bulk of total width $T = 1$ μm, aptly modeling an ionization continuum in which the electron can escape and be lost. The envelope functions in Fig. 1(a) have been calculated using these parameters. To get large values of the coupling with a single quantum well, we consider the electronic transition coupled to a subwavelength photonic resonance with an effective cavity length L_c much smaller than the transition wavelength λ. In particular, we fix $L_c = 25$ nm, which for a photonic transition quasi-resonant to the frequency of first ionization χ, implies $\frac{\lambda}{2L_c} \simeq 125$, a value that can be today achieved using various mid-infrared architectures [51–53]. Note that specific implementations could impose further constraints on the shape of the bulk (e.g., forcing the quantum well to be at a specific distance from one of the boundaries), but for the sake of definiteness we will neglect this possibility and consider the quantum well to be placed in the center of the 1 μm bulk. A microscopic model for the photonic resonator is instead considered for the case of multiple quantum wells described below.

In Figs. 2–4 we show the results for cavity energies $\hbar\omega_q^a = 185, 195$, and 205 meV respectively. In panel (a) of each figure we plot the polaritonic spectrum as a function of the doping, clearly showing the ionization continuum around $\hbar\chi = 188.4$ meV. In the case $\omega_q^a < \chi$, a single discrete mode below the continuum is also present for any doping. In the case of $\omega_q^a > \chi$, it is present only above a critical doping, since the coupling needs to be strong enough to push a polaritonic mode out of the continuum. In panels (b) we instead plot the normalized excited electronic density $|\psi_{sq}^e(z)|^2$ for the lowest-lying polaritonic state in a neighborhood of the quantum well. Since we are considering a quantum well with a single initially occupied electronic state, the ground wavefunction $\psi_{sq}^g(z)$ coincides with the lowest subband envelope function and thus depends neither on s nor on doping. In Fig. 5(a) we plot the ground density $|\psi_{sq}^g(z)|^2$ (blue solid line) and the excited density $|\psi_{sq}^e(z)|^2$ (red dashed line) corresponding to the lowest eigenmode in Fig. 3(g) in a 40 nm interval around the quantum well.

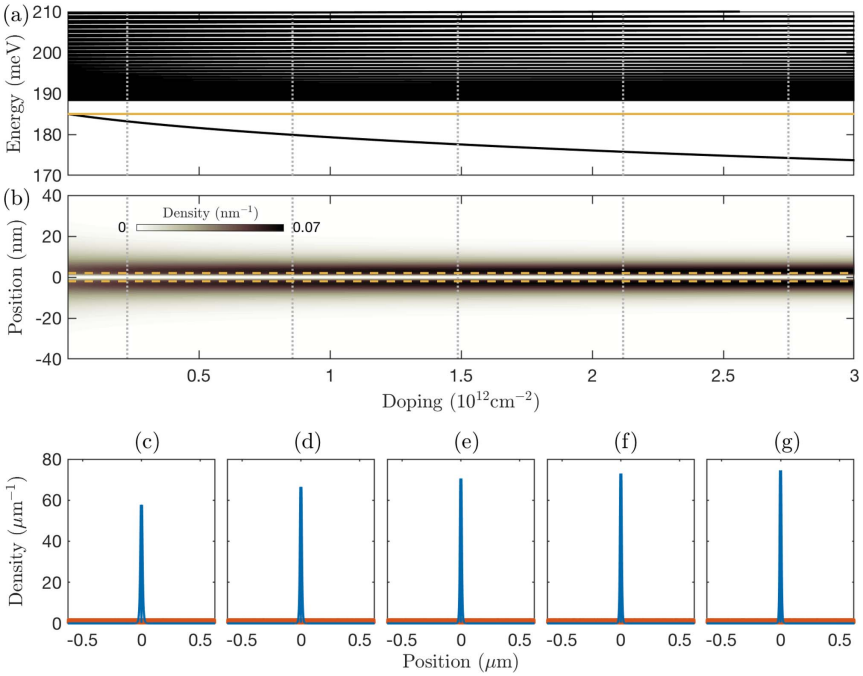

Fig. 2. Simulation of a single quantum well of width $L_{\mathrm{QW}} = 4$ nm in a bulk of total width $T = 1$ μm, with effective cavity length $L_c = 25$ nm and cavity energy $\hbar\omega_q^a = 185$ meV, smaller than the first ionization $\hbar\chi = 188.4$ meV. (a) Polaritonic spectrum as a function of the doping. The yellow line marks the cavity energy. (b) Colormap of the excited electron density $|\psi_{sq}^e(z)|^2$ for the lowest lying polaritonic mode as a function of doping. Yellow dashed lines mark the boundaries of the quantum well. (c)–(g) Plots of $|\psi_{sq}^e(z)|^2$ for all the polaritonic modes (all the s up to the cutoff) relative to the five values of doping marked by dotted vertical gray lines in panels (a) and (b). The lowest lying mode represented in panel (b) is plotted in blue; all the other modes in the continuum are instead in red, forming the thin homogeneous red band of density T^{-1} visible at the bottom of each panel. Note that, due to the different scale, the node in the localized excited electronic density visible in panel (b) is not clearly resolved in panels (c)–(g).

We can verify that a bound exciton forms only when a discrete polaritonic resonance below the continuum is present. The difference between the energy of first ionization and the energy of the discrete polaritonic mode plays in this case the role of binding energy for the exciton, being the excess energy the matter component of the polariton needs to dissociate into the continuum. By comparing Figs. 2–4, we can thus realize that the binding energy depends non-trivially on both the strength of the

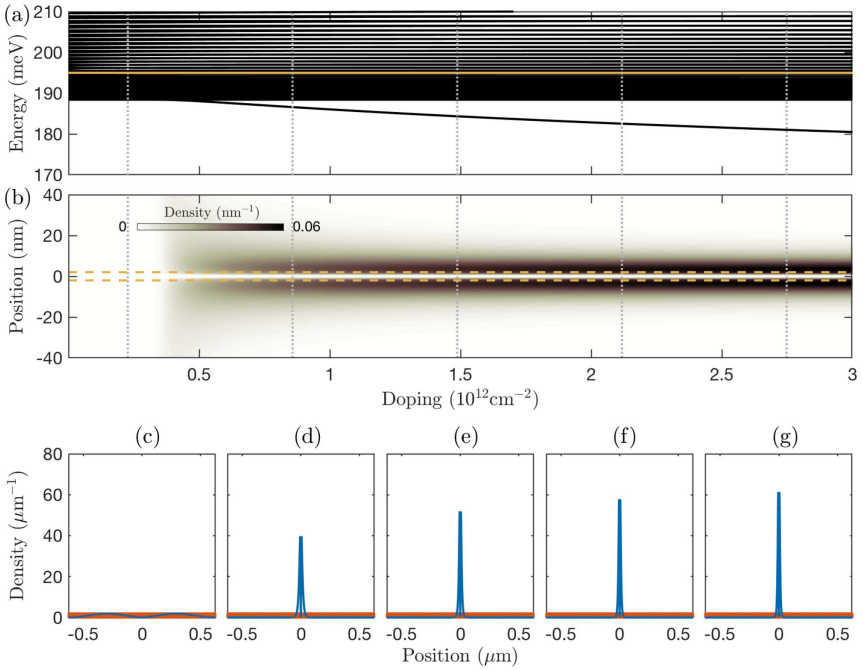

Fig. 3. Same as in Fig. 2, but with cavity energy $\hbar\omega_q^a = 195$ meV, larger than the first ionization $\hbar\chi = 188.4$ meV.

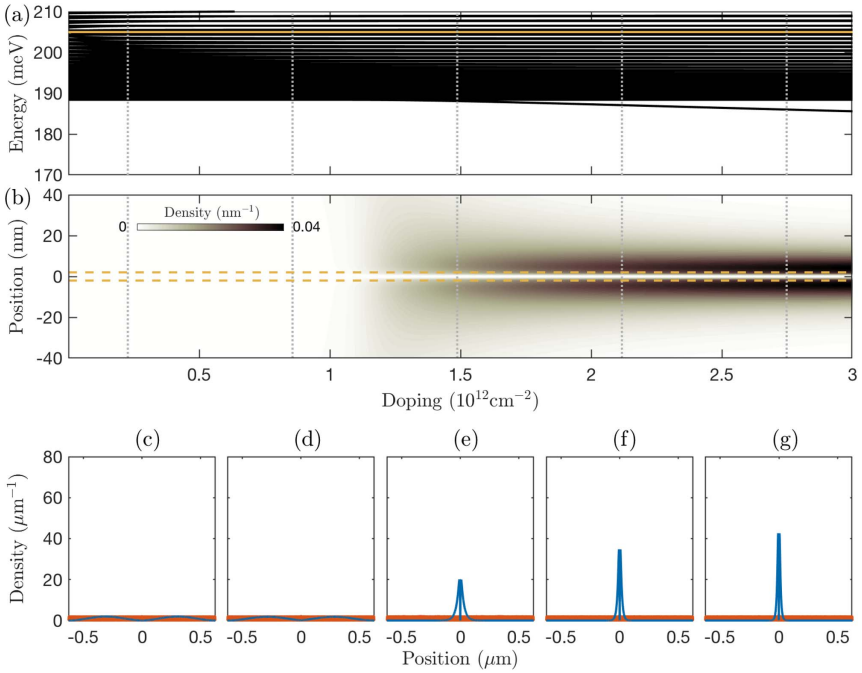

Fig. 4. Same as in Fig. 2, but with cavity energy $\hbar\omega_q^a = 205$ meV, larger than the first ionization $\hbar\chi = 188.4$ meV.

light–matter interaction and on the detuning between the cavity mode and the edge of the continuum. At low enough temperature, the discrete polaritonic resonance, not having enough energy to decay in the ionization continuum, is thus expected to have a linewidth of the order of few meV, determined by non-parabolicity, electron–phonon, and electron–electron scattering [54], as well as by the coupling of its photonic component to extra-cavity radiative modes. The predicted coupling-induced shifts are thus sizably larger than the expected linewidths, making those resonances spectroscopically observable and individually addressable.

To prove that bound excitonic states do not exist in the continuum below the critical density, in panels (c)–(g) of Figs. 2–4 we plot the excited electronic density $|\psi^e_{sq}(z)|^2$ for all the polaritonic modes, using a cutoff of 500 meV on the single electron energies. Lines corresponding to all values of s except the lowest-lying one are all plotted in red, and their overlap forms the uniform red band that can be seen on the very bottom of each panel, of homogeneous density T^{-1}. Such homogeneous density, vanishing in the limit $T \to \infty$ of a true continuum, is that expected from a standard bound-to-continuum excitation. The density of the first mode is instead plotted in blue. Those results further confirm that a bound exciton is present only when a discrete polaritonic mode appears. Note that due to the different scales of panels (b) and (c)–(g) the node of the excited density is not clearly visible in the latter.

Of course the normalized electronic densities give only partial information on the existence and observability of resonator-induced bound exciton states, because from Eq. (8) they are weighted by the matter fraction P_{sq}. In Fig. 5(b) we thus plot P_{sq} relative to the mode plotted in panels (b) of Figs. 2–4 as a function of doping, for the three considered values of the cavity energy. As expected, when the bare cavity mode is below the continuum ($\hbar\omega_q^a = 185$ meV, blue solid line), the discrete lowest-lying polaritonic mode for a vanishing doping is just the bare cavity with a vanishing matter component. In the opposite cases ($\hbar\omega_q^a = 195$ meV, red dashed line, and $\hbar\omega_q^a = 205$ meV yellow dashed–dotted line) the lowest mode is initially purely matter ($P_{sq} = 1$), and only when the discrete polaritonic mode appears do we observe light–matter hybridization. In all three cases, though, a strong hybridization is observed for experimentally achievable values of the doping.

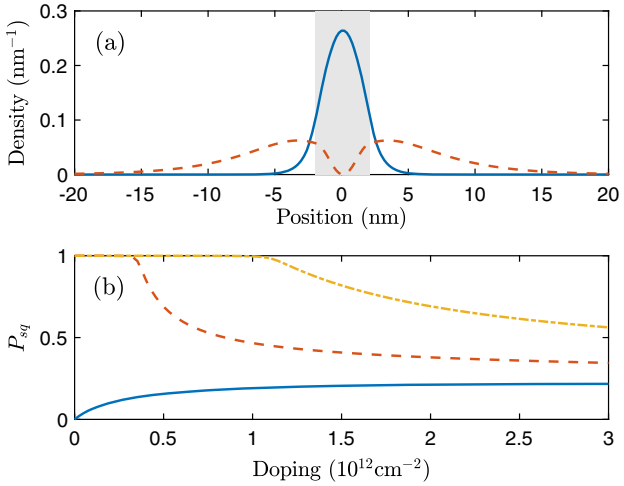

Fig. 5. (a) Ground (blue solid line) and excited (red dashed line) electronic densities corresponding to the lowest eigenmode in Fig. 3(g). The shaded region corresponds to the quantum well. (b) Weight of the matter component P_{sq} for the lowest-lying polaritonic mode as a function of doping for $\hbar\omega_q^a = 185$ meV (blue solid line), $\hbar\omega_q^a = 195$ meV (red dashed line), and $\hbar\omega_q^a = 205$ meV (yellow dashed–dotted line). Other parameters as in Fig. 2.

B. $n_{QW} = 20$

Having investigated the single-quantum-well case, and demonstrated the formation of bound excitonic resonances for suitable

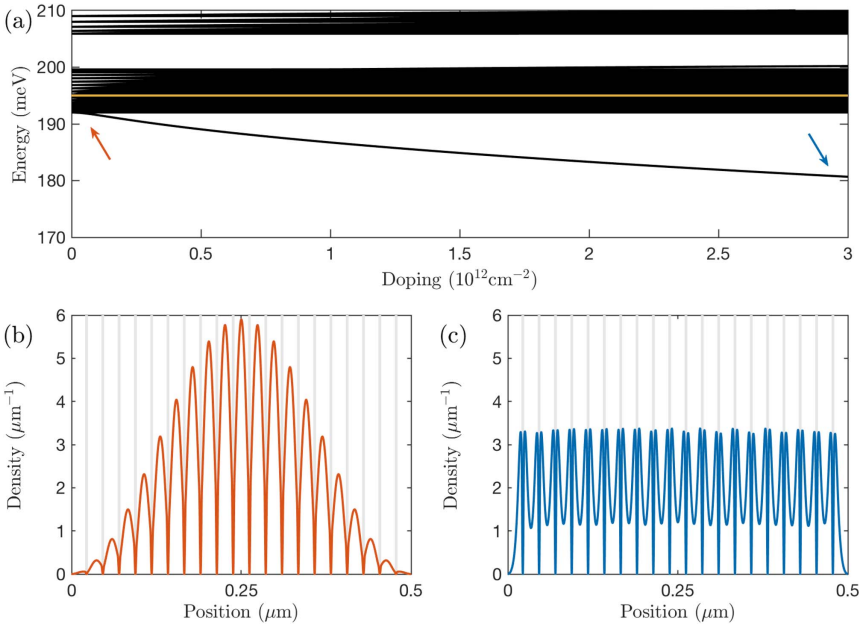

Fig. 6. Simulation of $n_{\mathrm{QW}} = 20$ quantum wells of width $L_{\mathrm{QW}} = 4$ nm in a bulk of total width $T = 0.5$ μm embedded in a planar microcavity. The TM0 mode of the microcavity is chosen to have energy $\hbar\omega_q^a = 195$ meV, larger than the first ionization energy $\hbar\chi = 192$ meV. (a) Polaritonic spectrum as a function of the doping. The yellow line marks the cavity energy. (b), (c) Plots of the excited electron density $|\psi_{sq}^e(z)|^2$ for the lowest-lying polaritonic mode, for values of doping equal, respectively, to $N_{\mathrm{2DEG}} = 0$ and 3×10^{16} cm^{-2}, marked by arrows in panel (a). Shaded regions correspond to the locations of the quantum wells.

strength of the light–matter interaction, here we will consider the case of $n_{\mathrm{QW}} = 20$ quantum wells that couple to the TM0 mode of a planar resonator as wide as the electron bulk. The relative facility to achieve strong coupling in multiple-quantum-well structures [29–31] will allow for a rapid observation of the discrete polaritonic resonances emerging out of the continuum, heralding the generation of resonator-induced bound excitonic states.

We consider a sample with $n_{\mathrm{QW}} = 20$ quantum wells, separated by barriers of 20 nm, with the same length $L_{\mathrm{QW}} = 4$ nm used previously, and the bulk and the resonator have a total length $L_c = T = 0.5$ μm. The filling factor $n_{\mathrm{QW}} L_{\mathrm{QW}}/L_c = 0.16$, which in Ref. [47] was shown to be the relevant figure of merit to quantify the strength of the light–matter interaction, is thus the same as in Section 3.A, allowing for a meaningful comparison.

In Fig. 6(a) we plot the eigenmodes for $\hbar\omega_q^a = 195$ meV. Notwithstanding minor differences, including a larger energy of first ionization $\hbar\chi = 192$ meV, which are to be expected given the different structure of the continuum, we recover results in agreement with those in Fig. 3(a), showing that discrete resonances below the continuum are observable also in multi-quantum-well structures. In Figs. 6(b) and 6(c) we plot the excited electronic density in the lowest-lying eigenmode, for values of the doping $N_{\mathrm{2DEG}} = 0$ and 3×10^{12} cm^{-2}, respectively, marked by arrows in Fig. 6(a). It can be observed that the electronic densities for the continuous (red) and discrete (blue) modes are not as spectacularly different as in Fig. 3. This was expected because, in a multi-quantum-well structure, ionized electrons will still be confined in the proximity of quantum wells, as the total space occupied by the quantum wells is now a macroscopic fraction of the total width of the bulk. Nevertheless, we can recognize the same physics at play, as the collective density, although modulated by the presence of the quantum wells, passes from a mode of the entire structure, whose intensity is maximal at the center, to a bound one in which the density is roughly the same in each quantum well.

Finally, with the objective of testing the accuracy of our quantum theory and to provide an experimentally accessible observable, we calculated the reflectivity of the same structure

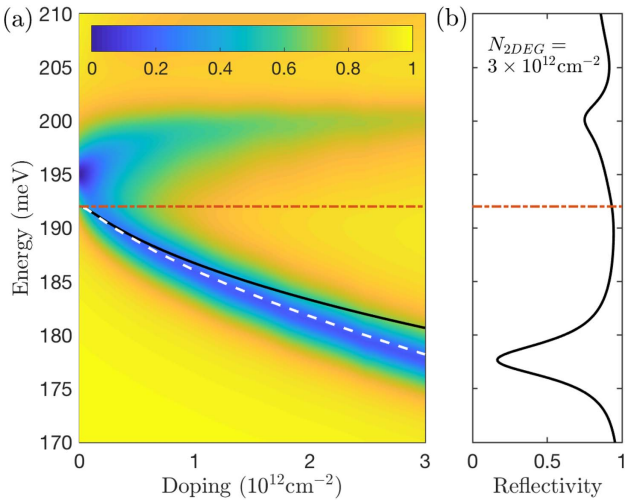

Fig. 7. (a) Reflectivity map for the same structure studied in Fig. 6, calculated considering an electronic linewidth of 4 meV. The horizontal dashed–dotted red line marks the first ionization energy. The solid black and dashed white lines mark instead the dispersion of the lowest polariton mode obtained using the Hopfield approach, respectively without and with the effective medium approximation. (b) A vertical cut of panel (a) for $N_{\mathrm{2DEG}} = 3 \times 10^{12}$ cm^{-2}.

coupled to a planar metallic resonator, using a classical transfer matrix approach in the effective medium approximation including local field effects [39,55] and considering an electronic linewidth of 4 meV. Results are shown in Fig. 7, which replicates acceptably well the modal spectrum of Fig. 6(a). Superimposed on the reflectivity map we plot, with a solid black line, the lowest-lying polariton from Fig. 6(a). The small difference between the Hopfield and transfer matrix approaches, visible in the increased redshift of the reflectivity dip corresponding to the discrete polariton mode in the transfer matrix results, is due to the use of an effective medium approximation. We verified the origin of such a discrepancy by implementing the same approximation in the Hopfield model, as described in Ref. [47] and explained in Supplement 1, leading to the dashed white line, which instead correctly follows the reflectance dip up to high levels of doping.

4. CONCLUSIONS

In this work we demonstrated that an ionizing electronic transition can be strongly coupled to a photonic resonator. Spectroscopically this strong coupling manifests itself with the appearance of a discrete optically active resonance below the ionization threshold. Electronically such a discrete resonance corresponds to the generation of bound excitonic states. In contrast to the Coulomb interaction responsible for electron–hole binding in usual excitons, the bound state anticipated in this work relies on a novel mechanism due to the coupling with the cavity-photonic field.

The natural next question then is how the existence of these states can be directly probed. From the optical side, the width and the shape of the resonance bears the typical signatures of localization. For instance, the absorption of a bound-to-continuum transition has a large and asymmetric shape, while a bound-to-bound transition is narrower (typically below 10% at room temperature) and Lorentzian shaped (see, for example, Ref. [40]). However, a truly direct way to prove the electronic localization effect would require electrical measurements. One possibility is to use scanning tunnel microscopy. An interesting alternative that can open up vaster perspectives in the long term is to develop quantum-well (QWIP) or quantum cascade (QCD) intersubband detectors operating in strong coupling. Such devices rely on polaritonic excitations tunneling out into electronic states: the study of the transport in such devices can directly prove an electronic localization effect.

Our results can find direct applications in the physics and technology of intersubband transitions in doped quantum wells, where the potential of exploiting bound-to-continuum transitions [56,57] and of cavity-induced modifications of electronic states [38] were already recognized. More broadly, this investigation, which could be extended to other cavity quantum electrodynamics systems in both solid-state and atomic physics, demonstrates a novel way strong coupling can be exploited to influence the properties of materials coupled to light, with potential impact on fields ranging from chemistry to material science.

Funding. FP7 Ideas: European Research Council (IDEAS-ERC) (GEM 306661); European Union FET (Open Grant MIR-BOSE 737017); Engineering and Physical Sciences Research Council (EPSRC) (EP/M009122/1); Provincia Autonoma di Trento; Royal Society (University Research Fellowship).

Acknowledgment. The authors thank Prof. J. Khurgin for useful comments on the interpretation of the results.

See Supplement 1 for supporting content.

REFERENCES

1. A. V. Kavokin, J. J. Baumberg, G. Malpuech, and F. P. Laussy, *Microcavities* (Oxford University, 2011).
2. S. De Liberato, "Light-matter decoupling in the deep strong coupling regime: the breakdown of the Purcell effect," Phys. Rev. Lett. **112**, 016401 (2014).
3. A. Bayer, M. Pozimski, S. Schambeck, D. Schuh, R. Huber, D. Bougeard, and C. Lange, "Terahertz light-matter interaction beyond unity coupling strength," Nano Lett. **17**, 6340–6344 (2017).
4. N. C. Passler, C. R. Gubbin, T. G. Folland, I. Razdolski, D. S. Katzer, D. F. Storm, M. Wolf, S. De Liberato, J. D. Caldwell, and A. Paarmann, "Strong coupling of epsilon-near-zero phonon polaritons in polar dielectric heterostructures," Nano Lett. **18**, 4285–4292 (2018).
5. S. Savasta, O. Di Stefano, V. Savona, and W. Langbein, "Quantum complementarity of microcavity polaritons," Phys. Rev. Lett. **94**, 246401 (2005).
6. A. Le Boité, M.-J. Hwang, H. Nha, and M. B. Plenio, "Fate of photon blockade in the deep strong-coupling regime," Phys. Rev. A **94**, 033827 (2016).
7. L. Garziano, A. Ridolfo, S. De Liberato, and S. Savasta, "Cavity QED beyond rotating wave approximation: photon bunching from the emission of individual dressed qubits," ACS Photon. **4**, 2345–2351 (2017).
8. C. S. Muñoz, E. del Valle, A. G. Tudela, K. Müller, S. Lichtmannecker, M. Kaniber, C. Tejedor, J. J. Finley, and F. P. Laussy, "Emitters of N-photon bundles," Nat. Photonics **8**, 550–555 (2014).
9. I. Carusotto and C. Ciuti, "Quantum fluids of light," Rev. Mod. Phys. **85**, 299–366 (2013).
10. C. Gubbin and S. De Liberato, "Theory of nonlinear polaritonics: $X^{(2)}$ scattering on a β-SiC surface," ACS Photon. **4**, 1381–1388 (2017).
11. J. Galego, F. J. Garcia-Vidal, and J. Feist, "Cavity-induced modifications of molecular structure in the strong coupling regime," Phys. Rev. X **5**, 041022 (2015).
12. J. A. Cwik, P. Kirton, S. De Liberato, and J. Keeling, "Self-consistent molecular adaptation induced by strong coupling," Phys. Rev. A **93**, 033840 (2016).
13. E. Cortese, P. G. Lagoudakis, and S. De Liberato, "Collective optomechanical effects in cavity quantum electrodynamics," Phys. Rev. Lett. **119**, 043604 (2017).
14. H. L. Luk, J. Feist, J. J. Toppari, and G. Froenhof, "Multiscale molecular dynamics simulations of polaritonic chemistry," J. Chem. Theory Comput. **13**, 4324–4335 (2017).
15. J. Flick, H. Appel, M. Ruggenthaler, and A. Rubio, "Cavity Born-Oppenheimer approximation for correlated electron-nuclear-photon systems," J. Chem. Theory Comput. **13**, 1616–1625 (2017).
16. J. Keeling and P. G. Kirton, "Orientational alignment in cavity quantum electrodynamics," Phys. Rev. A **97**, 053863 (2018).
17. J. B. Khurgin, "Excitonic radius in the cavity polariton in the regime of very strong coupling," Solid State Commun. **117**, 307–310 (2001).
18. D. S. Citrin and J. B. Khurgin, "Microcavity effect on the electron-hole relative motion in semiconductor quantum wells," Phys. Rev. B **68**, 205325 (2003).
19. S. Brodbeck, S. De Liberato, M. Amthor, M. Klaas, M. Kamp, L. Worschech, C. Schneider, and S. Höfling, "Experimental verification of the very strong coupling regime in a GaAs quantum well microcavity," Phys. Rev. Lett. **119**, 027401 (2017).
20. E. Orgiu, J. George, J. A. Hutchison, E. Devaux, J. F. Dayen, B. Doudin, F. Stellacci, C. Genet, J. Schachenmayer, C. Genes, G. Pupillo, P. Samorì, and T. W. Ebbesen, "Conductivity in organic semiconductors hybridized with the vacuum field," Nat. Mater. **14**, 1123–1129 (2015).
21. J. Feist and F. J. Garcia-Vidal, "Extraordinary exciton conductance induced by strong coupling," Phys. Rev. Lett. **114**, 196402 (2015).
22. D. Hagenmüller, S. Schütz, J. Schachenmayer, C. Genes, and G. Pupillo, "Cavity-assisted mesoscopic transport of fermions: coherent and dissipative dynamics," Phys. Rev. B **97**, 205303 (2018).
23. G. L. Paravicini-Bagliani, F. Appugliese, E. Richter, F. Valmorra, J. Keller, M. Beck, N. Bartolo, C. Rössler, T. Ihn, K. Ensslin, C. Ciuti,

G. Scalari, and J. Faist, "Magneto-transport controlled by Landau polariton states," Nat. Phys. **15**, 186–190 (2019).
24. J. A. Hutchison, T. Schwartz, C. Genet, E. Devaux, and T. W. Ebbesen, "Modifying chemical landscapes by coupling to vacuum fields," Angew. Chem. **124**, 1624–1628 (2012).
25. F. Herrera and F. C. Spano, "Cavity-controlled chemistry in molecular ensembles," Phys. Rev. Lett. **116**, 238301 (2016).
26. L. A. Martínez-Martínez, M. Du, R. F. Ribeiro, S. Kéna-Cohen, and J. Yuen-Zhou, "Polariton-assisted singlet fission in acene aggregates," J. Phys. Chem. Lett. **9**, 1951–1957 (2018).
27. M. Ruggenthaler, J. Flick, C. Pellegrini, H. Appel, I. V. Tokatly, and A. Rubio, "Quantum-electrodynamical density-functional theory: bridging quantum optics and electronic-structure theory," Phys. Rev. A **90**, 012508 (2014).
28. J. Flick, M. Ruggenthaler, H. Appel, and A. Rubio, "Atoms and molecules in cavities, from weak to strong coupling in quantum-electrodynamics (QED) chemistry," Proc. Natl. Acad. Sci. USA **114**, 3026–3034 (2017).
29. D. Dini, R. Köhler, A. Tredicucci, G. Biasiol, and L. Sorba, "Microcavity polariton splitting of intersubband transitions," Phys. Rev. Lett. **90**, 116401 (2003).
30. A. A. Anappara, S. De Liberato, A. Tredicucci, C. Ciuti, G. Biasiol, L. Sorba, and F. Beltram, "Signatures of light-matter excitations in the ultra-strong coupling regime," Phys. Rev. B **79**, 201303 (2009).
31. Y. Todorov, A. M. Andrews, R. Colombelli, S. De Liberato, C. Ciuti, P. Klang, G. Strasser, and C. Sirtori, "Ultrastrong light-matter coupling regime with polariton dots," Phys. Rev. Lett. **105**, 196402 (2010).
32. S. De Liberato and C. Ciuti, "Stimulated scattering and lasing of intersubband cavity polaritons," Phys. Rev. Lett. **102**, 136403 (2009).
33. S. De Liberato, C. Ciuti, and C. C. Phillips, "Terahertz lasing from intersubband polariton-polariton scattering in asymmetric quantum wells," Phys. Rev. B **87**, 241304 (2013).
34. R. Colombelli and J.-M. Manceau, "Perspectives for intersubband polariton lasers," Phys. Rev. X **5**, 011031 (2015).
35. J.-M. Manceau, N.-L. Tran, G. Biasiol, T. Laurent, I. Sagnes, G. Beaudoin, S. De Liberato, I. Carusotto, and R. Colombelli, "Resonant intersubband polariton-LO phonon scattering in an optically pumped polaritonic device," Appl. Phys. Lett. **112**, 191106 (2018).
36. A. A. Anappara and A. Tredicucci, "Electrical control of polariton coupling in intersubband microcavities," Appl. Phys. Lett. **87**, 051105 (2005).
37. G. Guenter, A. A. Anappara, J. Hees, G. Biasiol, L. Sorba, S. De Liberato, C. Ciuti, A. Tredicucci, A. Leitenstorfer, and R. Hubert, "Sub-cycle switch-on of ultrastrong light-matter interaction," Nature **458**, 178–181 (2009).
38. S. De Liberato and C. Ciuti, "Quantum theory of electron tunneling into intersubband cavity polariton states," Phys. Rev. B **79**, 075317 (2009).
39. M. Załużny, "Bound-free intraband absorption line shape in quantum-well structures," Solid State Commun. **79**, 1013–1016 (1991).
40. F. Capasso, C. Sirtori, J. Faist, D. L. Sivco, S.-N. G. Chu, and A. Y. Cho, "Observation of an electronic bound state above a potential well," Nature **358**, 565–567 (1992).
41. U. Fano, "Effects of configuration interaction on intensities and phase shifts," Phys. Rev. **124**, 1866–1878 (1956).
42. R. Houdré, R. P. Stanley, and M. Ilegems, "Vacuum-field Rabi splitting in the presence of inhomogeneous broadening: resolution of a homogeneous linewidth in an inhomogeneously broadened system," Phys. Rev. A **53**, 2711–2715 (1996).
43. J.-M. Manceau, G. Biasiol, N. L. Tran, I. Carusotto, and R. Colombelli, "Immunity of intersubband polaritons to inhomogeneous broadening," Phys. Rev. B **96**, 235301 (2017).
44. C. Ciuti, G. Bastard, and I. Carusotto, "Quantum vacuum properties of the intersubband cavity polariton field," Phys. Rev. B **72**, 115303 (2005).
45. N. Shammah, N. Lambert, F. Nori, and S. De Liberato, "Superradiance with local phase-breaking effects," Phys. Rev. A **96**, 023863 (2017).
46. D. De Bernardis, P. Pilar, T. Jaako, S. De Liberato, and P. Rabl, "Breakdown of gauge invariance in ultrastrong-coupling cavity QED," Phys. Rev. A **98**, 053819 (2018).
47. Y. Todorov and C. Sirtori, "Intersubband polaritons in the electrical dipole gauge," Phys. Rev. B **85**, 045304 (2012).
48. Y. Todorov, "Dipolar quantum electrodynamics of the two-dimensional electron gas," Phys. Rev. B **91**, 125409 (2015).
49. S. De Liberato and C. Ciuti, "Quantum theory of intersubband polarons," Phys. Rev. B **85**, 125302 (2012).
50. G. Bastard, *Wave Mechanics Applied to Semiconductor Heterostructures* (EDP Sciences, 1990).
51. A. Benz, S. Campione, S. Liu, I. Montaño, J. F. Klem, A. Allerman, J. R. Wendt, M. B. Sinclair, F. Capolino, and I. Brener, "Strong coupling in the sub-wavelength limit using metamaterial nanocavities," Nat. Commun. **4**, 2882 (2013).
52. J. D. Caldwell, O. J. Glembocki, Y. Francescato, N. Sharac, V. Giannini, F. J. Bezares, J. P. Long, J. C. Owrutsky, I. Vurgaftman, J. G. Tischler, V. D. Wheeler, N. D. Bassim, L. M. Shirey, R. Kasica, and S. A. Maier, "Low-loss, extreme subdiffraction photon confinement via silicon carbide localized surface phonon polariton resonators," Nano Lett. **13**, 3690–3697 (2013).
53. C. R. Gubbin, S. A. Maier, and S. De Liberato, "Theoretical investigation of phonon polaritons in SiC micropillar resonators," Phys. Rev. B **95**, 035313 (2017).
54. I. Waldmüller, J. Förstner, S.-C. Lee, A. Knorr, M. Woerner, K. Reimann, R. A. Kaindl, T. Elsaesser, R. Hey, and K. H. Ploog, "Optical dephasing of coherent intersubband transitions in a quasi-two-dimensional electron gas," Phys. Rev. B **69**, 205307 (2004).
55. M. Załużny and C. Nalewajko, "Coupling of infrared radiation to intersubband transitions in multiple quantum wells: the effective-medium approach," Phys. Rev. B **59**, 13043–13053 (1999).
56. J. Faist, M. Beck, and T. Aellen, "Quantum-cascade lasers based on a bound-to-continuum transition," Appl. Phys. Lett. **78**, 147–149 (2001).
57. G. Scalari, N. Hoyler, M. Giovannini, and J. Faist, "Terahertz bound-to-continuum quantum-cascade lasers based on optical-phonon scattering extraction," Appl. Phys. Lett. **86**, 181101 (2005).